

# **Rheo-NMR: A New Window on the Rheology of Complex Fluids**

Paul T. Callaghan

Volume 9, pp 737–750

in

Encyclopedia of Nuclear Magnetic Resonance

Volume 9: Advances in NMR

(ISBN 0471 49082 2)

Edited by

David M. Grant and Robin K. Harris

© John Wiley & Sons, Ltd, Chichester, 2002

# Rheo-NMR: A New Window on the Rheology of Complex Fluids

Paul T. Callaghan

Victoria University of Wellington, Wellington, New Zealand

---

1	Introduction	1
2	Micro-Imaging and NMR Velocimetry	2
3	Applications of Rheo-NMR	4
4	Conclusions	12
5	References	13

---

## 1 INTRODUCTION

Over the past decade, NMR has made a significant impact in chemical engineering, where it is being extensively used for the non-invasive study of dispersion and flow in porous media. Now it is finding effective use in the study of the mechanical properties of complex fluids. At the heart of that development is the dual capacity of NMR to provide information at the microscopic level regarding molecular organization and dynamics, and at the macroscopic level regarding the local rate of fluid deformation. It is the combination of the various tools of NMR spectroscopy with those of NMR imaging, and velocimetry that makes this dualism possible.

### 1.1 Complex Fluids and Rheology

We tend to think of condensed matter as sub-dividing into the two basic phases of solid and liquid. When subjected to a stress a solid will deform by a fixed amount and store energy elastically whereas a liquid flows and dissipates energy continuously in viscous losses. But many interesting materials in their condensed phase possess both solid and liquid-like properties. These include polymer melts and solutions, lyotropic and thermotropic liquid crystals, micellar surfactant phases, colloidal suspensions and emulsions. Most biological fluids, most food materials and many fluids important in industrial processing or engineering applications exhibit such complexity. Complex fluids manifest both an elastic and a viscous response, and they generally possess ‘memory’, which means that the stress which they exhibit at any moment will depend on their history of prior deformation. They tend to exhibit non-linear mechanical behavior, which means that their mechanical properties may change as the deformation increases, an effect that is generally attributed to molecular reorganization. And they invariably possess a wide range of characteristic time scales, from the rapid (ps to ns) local Brownian motion of small molecules or molecular

segments, to the very slow (ms to s) motions associated with the reorganization or reorientation of large molecular assemblies or macromolecules. The study of the mechanical properties of complex fluids is known as ‘rheology’,<sup>1</sup> a name which derives from the Greek word ‘rheo’ which means ‘to flow’.

Traditionally, rheology was a subject concerned principally with mechanical properties. Recently however attention has focused on trying to determine the molecular basis of complex mechanical properties. If we can better understand this basis then we can better design desirable fluidic properties, we can better process modern materials based on polymers and organized molecular states, we can better produce foods of the right texture, and we can better understand how nature works, for example in the way synovial fluid protects our joints, or in the way a spider can extrude a protein silk whose strength surpasses that of steel.

The interest in the molecular-mechanical link has led to the amalgamation of a number of spectroscopic and rheological techniques in which a flow or deformation cell is incorporated within the spectrometer detection system. Examples include the use of neutron scattering,<sup>2</sup> light scattering,<sup>3</sup> birefringence and dichroism techniques.<sup>4,5</sup> The most recent addition, NMR, has provided a number of new and valuable features. For example, it can be used to study materials which are optically opaque. The imaging capability of NMR means that it can be used to measure local velocity profiles and molecular densities directly. The wide-ranging spectroscopic tools available to NMR also make it possible to measure molecular order and dynamics.

### 1.2 History of Rheo-NMR

The earliest suggestion of the use of NMR methods to measure rheological properties was by Martins et al., in 1986.<sup>6</sup> These authors pointed out that physically reorienting a sample of a nematic liquid crystal inside the NMR magnet would lead to a slow evolution of the spectrum during subsequent director realignment, interpretation of which could yield information about rotational visco-elasticity. This first type of Rheo-NMR method was later applied by Goncalves et al.,<sup>7</sup> who used proton NMR spectra to monitor the magnetic field reorientation of an initially aligned sample of a nematic polymer liquid crystal, following the sudden physical rotation. By carefully fitting these spectra, rotational (Leslie) viscosities were calculated along with elastic constants associated with defect formation.

In 1990, Nakatani, Polliks and Samulski<sup>8</sup> described a quite different Rheo-NMR experiment in which the proton NMR spectrum of a polymer melt was investigated under shear. They acquired their signal from a 100 kD polydimethylsiloxane sample which was contained in the gap of a cone-and-plate cell located in the NMR electromagnet, and in which the cone was driven to produce a shear rate of  $4\text{ s}^{-1}$ . In this experiment the proton NMR spectrum broadened under shear and slowly relaxed once shearing ceased. In 1991, another approach to Rheo-NMR was reported by Xia and Callaghan (1991)<sup>9</sup> who showed that NMR microscopy could be used to measure shear-thinning effects in the semi-dilute solution of a high molecular weight polymer, in particular by observing the deviation from Poiseuille flow apparent when

the fluid was pumped through a narrow (700  $\mu\text{m}$  diameter) pipe. Then, in 1994, Grabowski and Schmidt<sup>10</sup> demonstrated the use of the deuterium quadrupole interaction to investigate molecular order in studying the alignment of nematic liquid crystalline directors under shear, finding the equilibrium angle in the competition between the magnetic torque and the shear. This type of experiment proved able to yield the ratio of specific Leslie viscosities to the magnetic anisotropy. A detailed review of the science of Rheo-NMR can be found in a recent chapter<sup>11</sup> in *Reports on Progress in Physics*. Here we will outline the basic principles, and give a few examples.

### 1.3 Heterogeneity and the Need for Spatial Localization

In rheological measurements a material is subject to deformation and the stress,  $\sigma(t)$ , is monitored as a function of the time dependent strain,  $\gamma(t)$ . Such measurements require the deformation of fluid under the influence of relative motion of the fluid with respect to containment surfaces, the source of the externally applied stress. A simple example is that of pipe flow, where a velocity gradient exists between the wall, at which the fluid is stationary, and the center of the pipe, at which the fluid velocity is a maximum. Alternatively, the fluid may be held in a cell whose containment surfaces themselves move, generally in rotation and under the influence of an externally applied torque. Typical geometries used for this purpose are the cone-and-plate cell, the concentric cylindrical Couette cell, and the four roll mill. A feature of all these systems is that the flow is heterogeneous, although in the case of the cone-and-plate, the stress, and hence the velocity gradient may be expected to be uniform. However, even where the stress is uniform, some classes of fluids will exhibit heterogeneous shearing.

One of the great advantages of NMR is that it may be used to image the velocity field within a rheological cell, thus providing non-invasive insight concerning the exact nature of deformational flow. The key to this approach is the use of NMR imaging, and in particular, imaging at microscopic resolution, since the containment cells are often of mm length scale. However, even where velocimetry is not the primary aim of the experiment, and one instead wishes to examine molecular properties via NMR spectroscopy, the heterogeneous nature of many flows dictate that one spatially localizes the acquired spectrum. In consequence the selective excitation or spectroscopic imaging methods of NMR microscopy<sup>12</sup> are demanded. Because of these factors, Rheo-NMR often requires a dual focus on NMR microscopy and NMR spectroscopy, the former giving insight at the mechanical length scale and the latter at the molecular length scale.

## 2 MICRO-IMAGING AND NMR VELOCIMETRY

### 2.1 Encoding for Position and Displacement

The basic principles governing NMR microscopy have been described in detail elsewhere.<sup>12</sup> A spin at position  $\mathbf{r}$ , in the presence of a magnetic field gradient,  $\mathbf{G}$ , will experience an additional local spin precession frequency,  $\gamma\mathbf{G}\cdot\mathbf{r}$ , thus acquiring a phase  $\exp(i\mathbf{k}\cdot\mathbf{r})$ ,  $\mathbf{k}$  being the reciprocal space dimension

conjugate to  $\mathbf{r}$  and given by  $\gamma\mathbf{G}t$ , where  $t$  is the evolution time. The nuclear spin density can be reconstructed by acquiring the complete signal over some appropriate volume of  $\mathbf{k}$  space and performing an inverse Fourier transformation, generally, in two dimensions using a plane of spins prepared by a frequency-selective excitation. The high spatial resolution needed for NMR microscopy depends on the use of large polarizing field ( $\geq 5$  T), small receiver coils of high sensitivity and gradient coils capable of delivering in excess of 20  $\text{G cm}^{-1}$ .

In order to image velocity we further encode the signal with a Pulsed Gradient Spin Echo (PGSE) pair.<sup>13,14</sup> These pulses define a second wave vector domain,  $\mathbf{q}$ , and impart a phase shift to the spins which depends directly on the motion of their parent molecules. In particular a spin moving by  $\mathbf{R} = \mathbf{r}' - \mathbf{r}$  over the time  $\Delta$  between the PGSE pulse pair acquires a phase factor  $\exp[i\mathbf{q}\cdot\mathbf{R}]$ . This contrast factor means that the signal acquired is effectively modulated both in  $\mathbf{k}$ - and  $\mathbf{q}$ -space. Double inverse Fourier transformation of the signal with respect to both  $\mathbf{k}$  and  $\mathbf{q}$  returns the local spin density  $\rho(\mathbf{r})$  as well as the function,  $\overline{P}_s(\mathbf{R}, \Delta)$ , which describes the ensemble distribution of molecular displacements for that location. Image analysis software<sup>14</sup> can be used to automatically process these distributions, using the width to

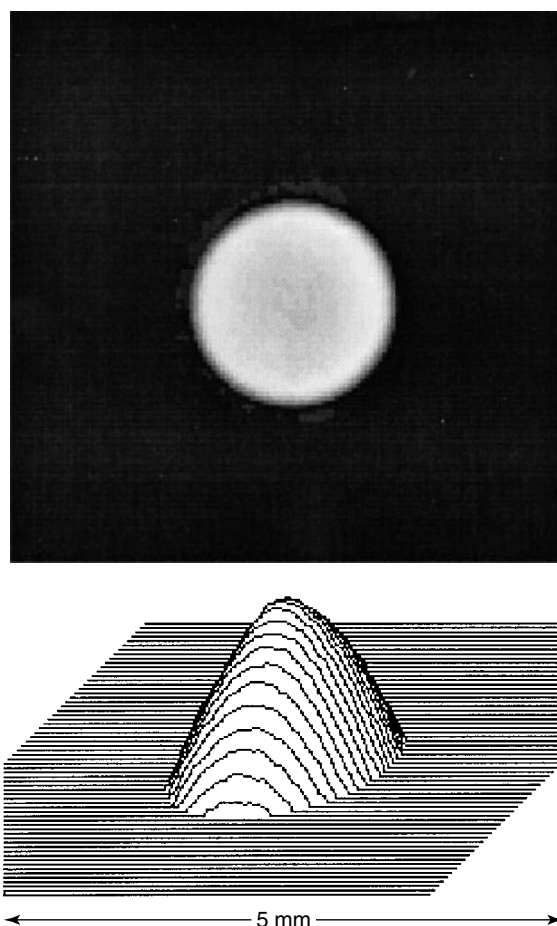


**Figure 1** NMR proton density image obtained at 60 MHz from a 1.9 mm ID capillary in which a surfactant solution is flowing. Also shown is a velocity map from the same capillary displayed as a stacked profile plot

estimate the rms Brownian motion  $(2D_s\Delta)^{1/2}$  and the mean displacement to estimate the flow. In this manner maps of  $D_s(\mathbf{r})$  and  $v(\mathbf{r})$  may be constructed. While the method depends on steady state flow conditions in the sample (a typical image will take several minutes to acquire), it does have the advantage of returning accurate and precise velocity maps. The sensitivity of the method is very high, enabling velocity resolution on the order of  $10\ \mu\text{m s}^{-1}$ . Figure 1 shows an image of the Poiseuille velocity field for fluid in laminar flow in a capillary.

## 2.2 Rheo-NMR Devices

Pipe flow methods, while suitable for fluids of low viscosity, have limited use for soft solids or highly viscous liquids where excessive pressure gradients may be needed to maintain the flow. Furthermore pipe flow suffers from the need to provide a sufficient volume of fluid to maintain an inlet reservoir. For viscous materials and for systems where only a small ( $<1\text{ g}$ ) quantity of fluid is available, it is necessary to use containment cells such as the cone-and-plate, cylindrical Couette, four roll mill and bi-axial extension cell. Figure 2 shows examples of such cells which fit within the rf coils of an NMR micro-imaging probehead.<sup>15</sup> All of these deformational flow devices can be driven by a drive shaft which sits in the bore of the magnet and which is turned by a stepper-motor gearbox assembly mounted above the magnet bore.

## 2.3 Spatially Localized Spectroscopy

In order to acquire an NMR spectrum from a selected region of a sample it is necessary to use one of two methods. In the first, known as spectroscopic imaging, the spectral property is independently encoded in an imaging experiment so that the spectrum can be reconstructed at every position. In the second, known as localized NMR spectroscopy, a frequency-selective RF pulse is applied in the presence of a magnetic

field gradient, so that only spins from a desired region of the sample participate in the NMR spectrum. The former approach is comprehensive but time consuming while the latter approach is the most efficient when the region from which the spectrum is desired is known in advance. Such localized spectroscopy is extensively used in biomedical magnetic resonance, where a wide variety of excitation methods are successfully employed.<sup>16,17</sup> One very effective spatial localization method is the composite soft/hard pulse 'selective storage' proposed by Post et al.<sup>18</sup> and first implemented by Aue et al.<sup>19</sup> This so-called 'split-sinc selective storage' consists of a  $\pi/2$  non-selective pulse sandwiched between the leading and trailing halves of a  $\pi/2$  sinc pulse of opposite phase. The relevant pulse sequence is shown in Figure 3. One of the advantages of this approach is that the desired slice magnetization is stored along the  $z$ -axis for later recall, while undesired magnetization is destroyed, thus making the method suitable as a 'front end' on any NMR sequence of interest. One such sequence might be a standard imaging routine (Figure 3a), so that it is possible to inspect and direct the chosen slice as required. Another advantage is the desired spins spend very little time in the transverse plane during the excitation process and thus suffer little  $T_2$  relaxation. The stored  $z$ -magnetization is subject only to the much less severe effects of longitudinal relaxation. An example of selective storage used for spectroscopy is shown in Figure 3(b) where a spin echo is used to encode in both the evolution ( $t_1$ ) and acquisition ( $t_2$ ) domains.

Figure 4 shows an application<sup>20</sup> of the selective storage sequence shown in Figure 3, in order to deliver magnetization from a selected slice across a cylindrical Couette cell. In the present instance, that magnetization is subsequently spatially encoding to produce the image shown. Having confirmed that this slice is as desired, the same excitation is then used as a precursor to a spectroscopy experiment in which the deuteron quadrupole interaction is measured. This experiment is discussed further in Section 3.3.

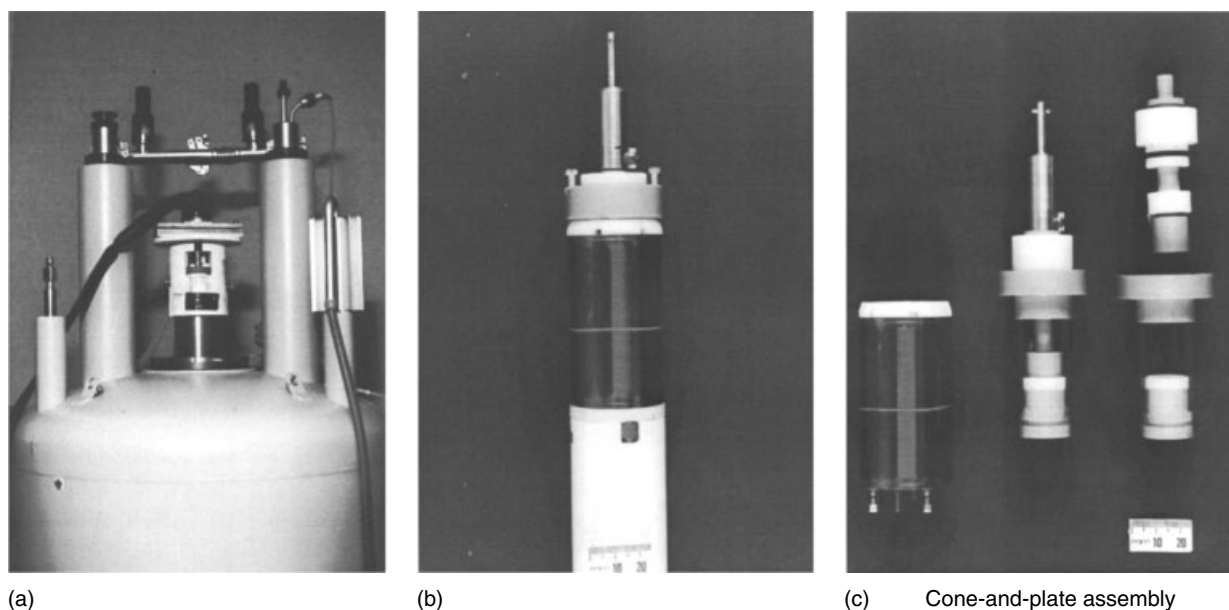


**Figure 2** (a) Superconducting standard widebore magnet with motor, driving shaft, (b) microimaging probehead and (c) cone-and-plate, rheometric device

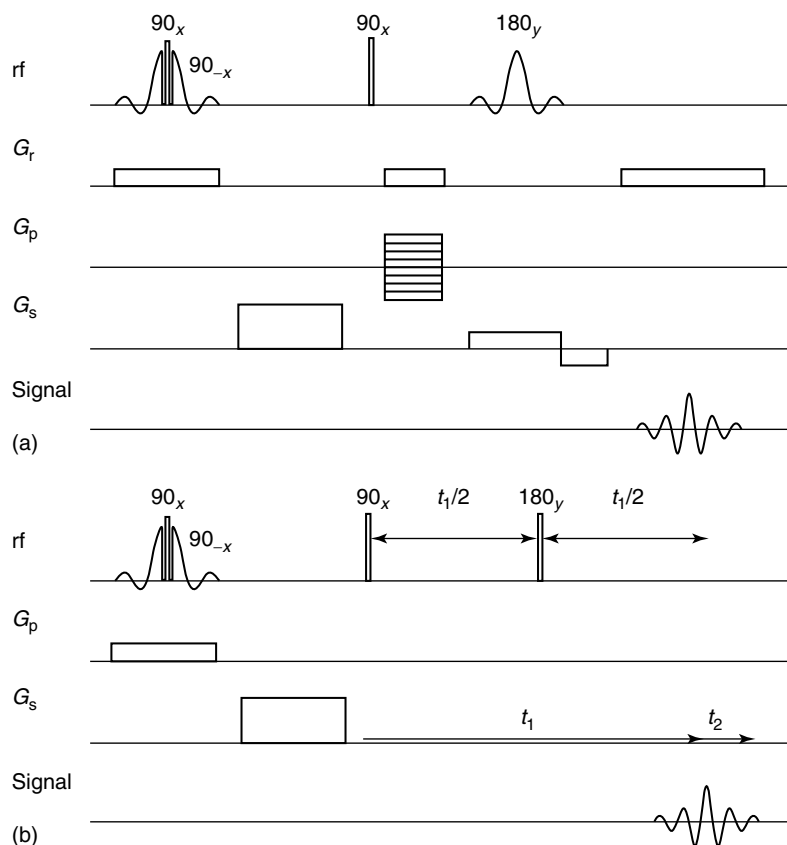


**Figure 3** Pulse sequences<sup>20</sup> showing two applications of the selective storage cluster followed by (a) an imaging module and (b) a two-dimensional spectroscopy module.  $G_p$ ,  $G_r$  and  $G_s$  are respectively the phase, read and slice gradients. The spoiler gradient shown here is applied along  $z$ , however it may equally be applied in any (or all) of the three orthogonal directions following the  $z$ -storage

### 3 APPLICATIONS OF RHEO-NMR

#### 3.1 Heterogeneous Flow and Shear Banding

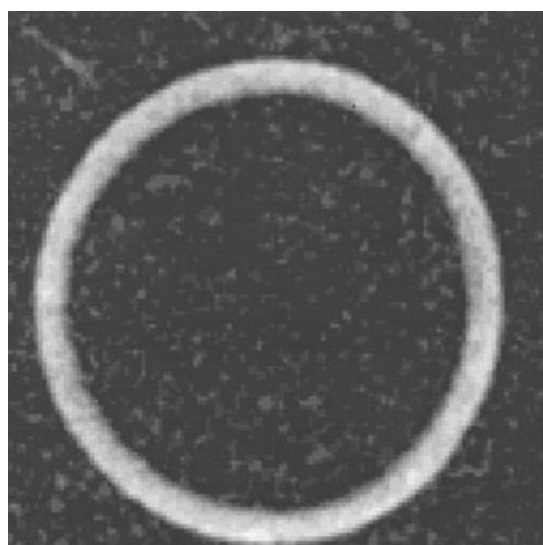
One important class of rheological measurement concerns the large strain response known as the ‘flow curve’ for which the stress is measured as a function of the rate of strain,  $\dot{\gamma} = \partial\gamma/\partial t$ , in a steady state shearing flow. Figure 5(a) shows examples of flow curves for different classes of materials, including Newtonian, shear thinning, shear thickening, and fluids exhibiting a yield stress.<sup>1</sup> The principal rheometric device for such measurement, the small angle cone-and-plate, is shown in Figure 5(b). In this device the stress is almost uniform, varying weakly as  $\text{cosec}^4\theta$  between the bottom plate ( $\theta = 90^\circ$ ) and the cone ( $\theta = 90^\circ - \alpha$ ) where  $\alpha$  is the cone angle, typically less than  $10^\circ$ . The strain rate  $\dot{\gamma} = \partial v_x/\partial y$  is assumed to be highly uniform since both the cone tangential velocity,  $v_x$ , and the gap are proportion to the local radius.

One of the most significant contributions of Rheo-NMR has been to show that the uniform shear-rate assumption may be violated in the case of certain classes of fluids in which pathological flow properties are exhibited. Figure 6 shows velocity maps and associated shear-rate maps<sup>21</sup> obtained for the wormlike surfactant system, cetylpyridinium chloride/sodium salicylate in water. While the velocity gradients show no deviation from uniformity at very low shear rates, above a certain critical value  $\dot{\gamma}_c$  we observe a dramatic variation in the rate-of-strain across the  $6^\circ$  cone gap in which a very high shear

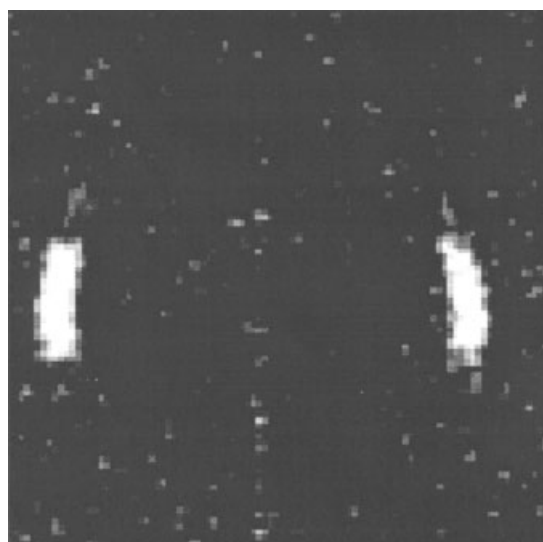
rate band exists at mid-gap (i.e., fixed angle  $\theta \approx 90^\circ - \alpha/2$ ) and independent of radius.

This shear banding phenomena explains the plateau in the flow curve. In the reptation reaction model of Cates,<sup>22</sup> the wormlike micelle system is predicted to exhibit a constitutive behavior as shown schematically in Figure 7 where the region of decreasing stress as the shear rate increases finds its origin in the reduction in entanglements as the worm chains align in the flow. This section of the flow curve is associated with unstable flow. Cates et al.<sup>23</sup> have suggested that because of the instability beyond the shear rate corresponding to the stress maximum,  $\sigma_c$ , in the schematic flow curve, separation of distinct shear bands may occur, in the manner of a first order phase separation. These bands will be associated with the intersections of a coexistence stress tie line with the upper and lower branches of the underlying flow curve and the proportions of each band will be as required to satisfy the average shear rate. That the NMR results are consistent with this picture is clear in Figure 8 where a series of profiles show that as the gap apparent shear rate is increased, the high shear rate band expands in width at approximately constant maximum shear rate rate.

Shear banding effects have apparently been seen in these materials via optical birefringence.<sup>24,25</sup> Birefringence effects are associated with anisotropic molecular alignment<sup>26</sup> and, as a consequence, the flow instability of the wormlike micelles have been associated with the onset of molecular ordering. NMR is also capable of investigating order and alignment



(a)



(b)

**Figure 4** (a) NMR image<sup>36</sup> obtained from protons at 300 MHz of a Couette cell containing the polymer PDMS in the 0.5 mm annular gap and (b) image of the same cell obtained following the selective storage sequence shown in Figure 3(a)

through utilizing inter-nuclear dipole interactions or nuclear quadrupole interactions. It is through the use of such spectroscopic approaches that Rheo-NMR holds the promise of further linking mechanical and molecular properties.

### 3.2 Nematic Ordering under Shear

By the use of deuterium labeling, it is possible to employ the deuterium quadrupole interaction to measure local order, since this interaction results in a two line NMR spectrum in which the splitting is proportional to the local order parameter, and to the alignment with respect to the magnetic field via the second rank Legendre Polynomial,  $P_2(\cos \theta) = (3 \cos^2 \theta - 1)/2$ .

We have used quadrupole interaction spectroscopy, along with spectroscopic imaging, to investigate<sup>27</sup> shear banding in

a wormlike micelle system in which birefringence banding had been observed (20% CTAB/D<sub>2</sub>O at 41 °C). Figure 9 shows the D<sub>2</sub>O <sup>2</sup>H NMR spectrum plotted as a function of radial position across the gap of a cylindrical Couette cell where the magnetic field is aligned with the vorticity axis. At the inner wall, where the stress is highest, a splitting is observed, indicative of a finite quadrupole interaction, while at the outer wall a single peak is observed. This data suggest the formation of a nematic phase at high stress and the transition to an isotropic phase, through a mixed phase region, at the region of low stress. What is particularly interesting about this experiment is that the associated velocity profile shows a banding in the shear rate which does not correlate simply with the local order parameters seen in the <sup>2</sup>H NMR spectra, indicating that the molecular ordering is associated with the monotonically varying stress, rather than the discontinuously varying rate of strain. The example provides valuable new insight regarding the origin of shear banding in systems close to an isotropic/nematic phase transition.

### 3.3 Shear-induced Director Rotation

Nematic liquid crystals under shear stress experience not only deformational flow but also director reorientation.<sup>28–31</sup> This process involves at least three independent rotational viscosities when describing the linear viscous response. In addition, the shear deformation results in the formation of complex defect structure which are governed by Frank elasticity effects<sup>32</sup> associated with director splay bend and twist. This defect structure is crucial to any understanding of the non-linear visco-elasticity of liquid crystals. A nice description of the linear viscous response is given by the theoretical treatment of Leslie and Ericksen,<sup>28–31</sup> who derived constitutive relations involving six independent coefficients,  $\mu_n$ . In this theory the Frank elasticity is ignored. A detailed description of Leslie-Ericksen theory is beyond the scope of this review and can be found elsewhere.<sup>33</sup>

In the context of Rheo-NMR, such nematic systems, which have intrinsic diamagnetic anisotropy, experience in addition a torque due to the magnetic field. Thus any deformation in the director field due to externally applied stress results in a competitive reorientation process. Two types of experiment involving such have been reported. The first is that performed by Martins and co-workers,<sup>6,7</sup> who rapidly rotated a sample of a nematic liquid crystal which had been previously aligned in the magnetic field. In a variety of experiments the subsequent relaxation of the director field back to equilibrium was monitored via the use of both proton and deuterium NMR. In the second type of experiment due to Schmidt and co-workers,<sup>10,34</sup> a nematic system has been continuously sheared in a cone-and-plate cell and the equilibrium direction orientation measured by use of the deuterium quadrupole interaction. The classes of material studied in this manner were thermotropic side-chain liquid crystal polymers, materials which present Leslie viscosities sufficiently large that significant alignment is possible at quite low shear rates, on the order of  $1 \text{ s}^{-1}$ . The rheometer used in these experiments incorporates a bottom plate which is free to rotate against a torsion spring, so that observation of the angular displacement gives a measure of the applied torque, and hence the stress applied to the fluid in the gap. As a consequence this Rheo-NMR device

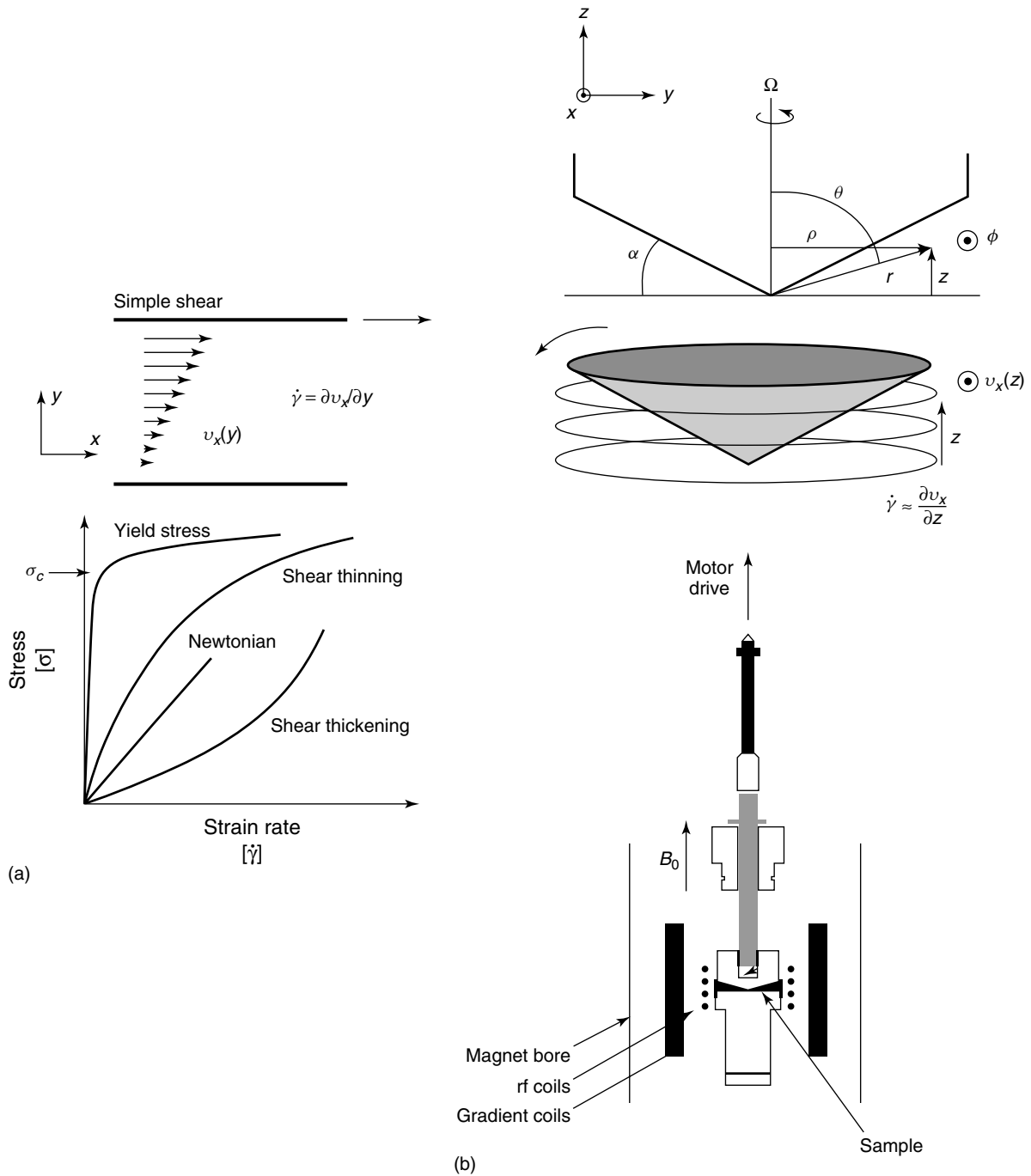


**Figure 5** (a) Schematic diagram of simple shear geometry and associated flow curves. (b) Cone-and-plate cell used to produce uniform stress and shear rate conditions along with the cone-and-plate Rheo-NMR device

allows additionally for simultaneous measurement for shear viscosity.

The steady-shear flow behavior of these nematic materials in the presence of a magnetic field,  $B_0$ , is nicely described using the Leslie-Ericksen theory. Under a shear rate  $\dot{\gamma}$  the director settles at an equilibrium angle to the magnetic field given by<sup>34</sup>

$$\tan \theta = \mp \frac{\chi_a B_0^2}{2\mu_0 |\mu_3| \dot{\gamma}} \pm \sqrt{\left( \frac{\chi_a B_0^2}{2\mu_0 |\mu_3| \dot{\gamma}} \right)^2 \pm \frac{|\mu_2|}{|\mu_3|}} \quad (1)$$

where  $\mu_2$  and  $\mu_3$  are Leslie coefficients, and  $\chi_a$  is the anisotropic part of the diamagnetic susceptibility tensor. The positive sign in the equation corresponds to a flow aligning ( $\mu_2/\mu_3 > 0$ ) nematic while the negative to a tumbling ( $\mu_2/\mu_3 < 0$ ) nematic. For a flow aligning system a stable angle is found for all shear rates, while for a tumbling nematic, a stable angle exists provided that  $\dot{\gamma}$  is sufficiently small that the term inside the square root sign is positive.

Siebert et al. have demonstrated these effects in an experiment on two different nematic systems.<sup>34</sup> The ‘flow-aligning’ system was a nematic side-chain polysiloxane obtained

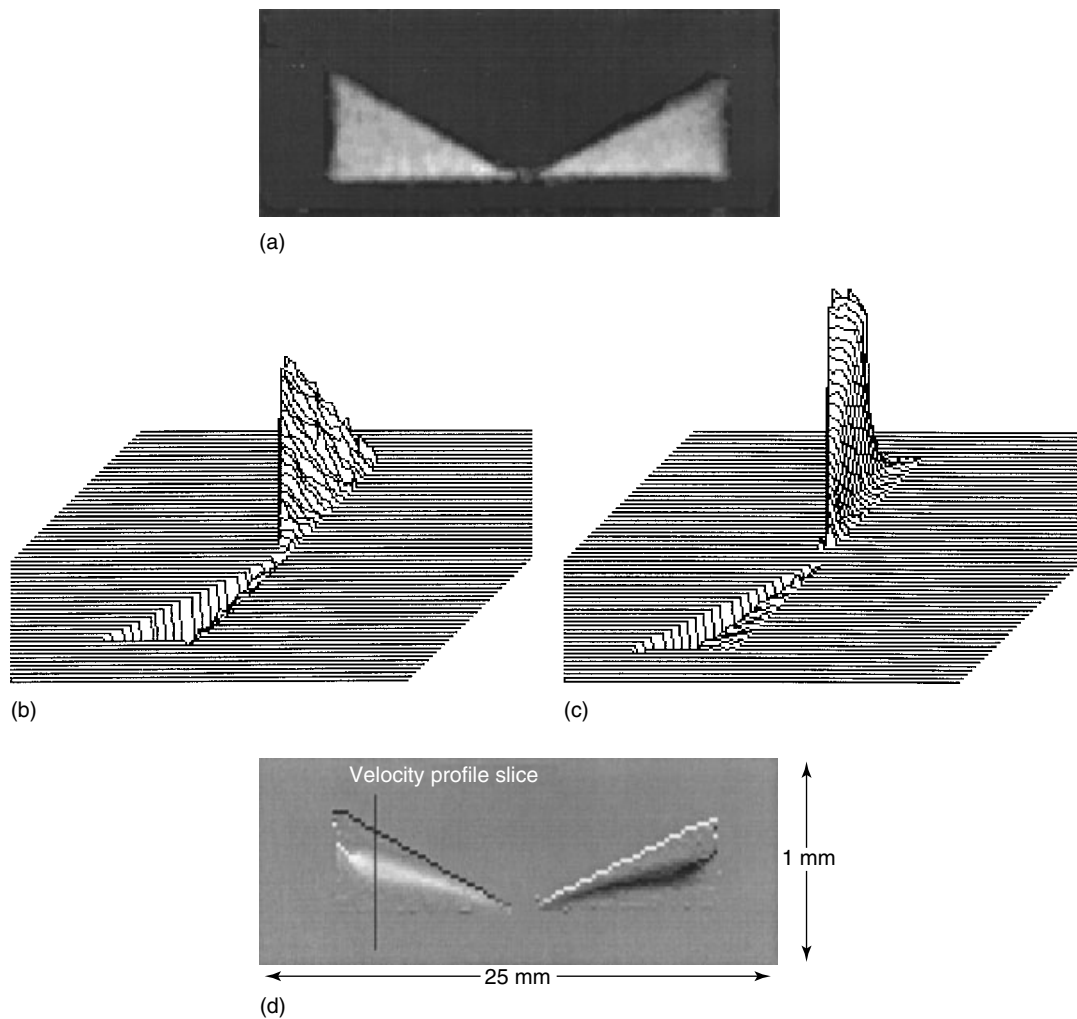


**Figure 6** (a) Proton density image obtained at 300 MHz for cetylpyridinium chloride/NaSal wormlike micelle solution in a  $7^\circ$  cone-and-plate cell (horizontal field of view 25 mm with vertical magnification expanded by a factor of 6). Data taken from Reference<sup>21</sup>. (b) Stacked profile plot showing velocity distribution across the gap at an apparent shear rate of  $1.5 \text{ s}^{-1}$ . (c) As for (b) but for  $16 \text{ s}^{-1}$ . (d) Image of shear rate distribution for cetylpyridinium chloride/NaSal wormlike micelle solution at an apparent shear rate,  $\omega/\tan \alpha$  of  $16 \text{ s}^{-1}$ , well beyond the critical shear rate and in an unstable region of the flow curve. Experimental shear rate profiles are taken along a line of approximately fixed radius as shown

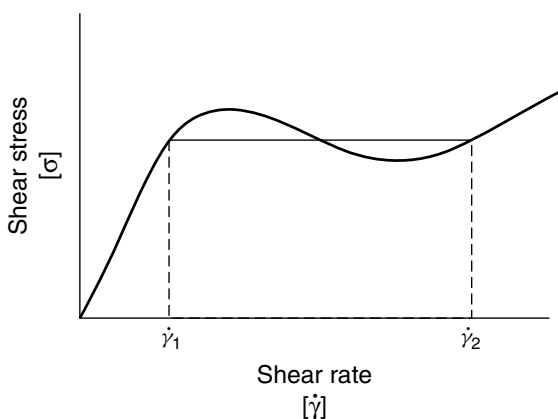


**Figure 7** Schematic flow curve for a fluid exhibiting double-valued stress vs rate-of-strain behavior. In the phase separation model for shear banding,<sup>23</sup>  $\dot{\gamma}_1$  and  $\dot{\gamma}_2$  correspond to coexisting shear rates at a single stress value

by the addition of 2,3,5,6-tetradeuterio-4-methoxyphenyl-4'-butenyloxybezoate to poly(hydrogen methyl siloxane), a material with a glass transition temperature of  $4^\circ\text{C}$  and a clearing point of  $97^\circ\text{C}$ . The experiment was performed at  $75^\circ\text{C}$  and deuterium NMR spectra were acquired at 46 MHz for a range of shear rates. These spectra are used to obtain the angle  $\theta$  from the quadrupole splitting  $\Delta v = AP_2(\cos \theta)$ , the constant  $A$  being determined from the splitting at zero shear. The splittings form an asymptote with increasing shear rate at a  $\theta$  value of around  $70^\circ$ . This angle, associated as it is with the dominance of mechanical torque over magnetic torque, corresponds to the alignment angle which would occur at all shear rates in the case of zero magnetic field.

The tumbling system was a mixture of 65% (w/w) poly{4-[4-(4-methoxyphenylazo)phenoxy]butylmethacrylate} in 4-tri-deuterio-methoxybenzoic acid-[4-*n*-hexoxyphenylester]. Corresponding spectra for three different temperatures were obtained in this system and, once again, a shear-rate dependent angle  $\theta$  was found associated with the competition between

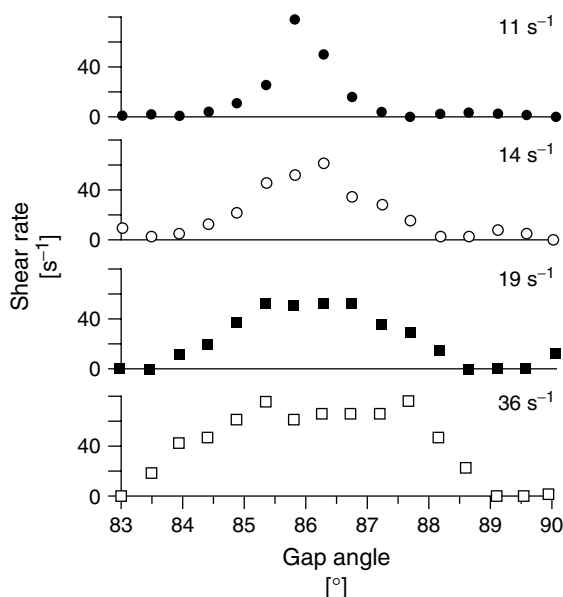


**Figure 8** Measured shear rate profiles<sup>21</sup> from for cetylpyridinium chloride/NaSal wormlike micelle solution along a line of approximately fixed radius (as shown in Figure 6) for the 7° cone-and-plate data of Figure 6, for 11 s<sup>-1</sup>, 14 s<sup>-1</sup>, 19 s<sup>-1</sup> and 36 s<sup>-1</sup>

the magnetic and mechanical torques. At shear rates beyond  $\theta \approx 50^\circ$ , no splitting could be found, a result consistent with the onset of director tumbling.

Figure 10 shows the respective alignment angles as a function of shear rates along with fits to the data using equation (1). In the case of the two different materials, opposite signs for  $\mu_2$  and  $\mu_3$  were necessary in order to reproduce the observed curvature of the data, confirming the respective flow aligning and tumbling character of the different polymer liquid crystals.

### 3.4 Shear-induced Deformation in Polymers

#### 3.4.1 Measurement of Segmental Alignment

Another intriguing correlation between shearing and molecular conformation has been investigated by Rheo-NMR. When a random coil polymer melt is subjected to shear, the polymer chain suffers a bi-axial deformation in which the principal axis of extension has a preferred orientation with respect to the hydrodynamic velocity direction.<sup>26</sup> The geometry is as indicated in Figure 11. As a result of the deformation, the chain entropy is reduced, leading to an increase in the Free Energy, the basis of the elastic response of the polymer melt.

The deformation may be usefully described by means of the averaged segmental alignment tensor<sup>26</sup>

$$S_{\alpha\beta}(t) = \left\langle \int_0^L ds u_\alpha(s, t) u_\beta(s, t) - \frac{1}{3} \delta_{\alpha\beta} \right\rangle \quad (2)$$

where  $\langle \dots \rangle$  represents the ensemble average and the integral is taken over the curvilinear path of  $s$  chain segments along the chain length  $L$ . In the Doi-Edwards formulation of entangled polymer dynamics<sup>26,35</sup> the stress tensor  $\sigma_{\alpha\beta}$  is

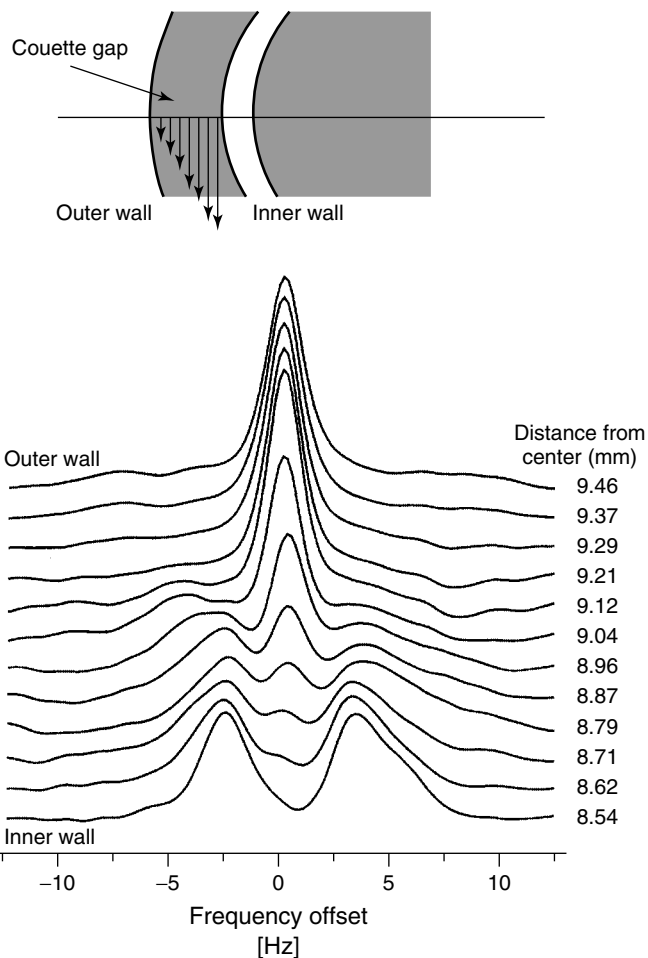


**Figure 9** <sup>2</sup>H NMR spectra obtained<sup>27</sup> at 46 MHz, from 20% w/w CTAB/D<sub>2</sub>O (41 °C) at different positions across the annular gap of a cylindrical Couette cell and at an apparent shear rate of 20 s<sup>-1</sup>. Near the inner wall, where the stress is highest, a quadruple splitting is observed, consistent with an ordered phase, while near the outer wall the single peak of an isotropic phase is seen. In between a mixed phase region exists

shown to be directly proportional to the average alignment tensor  $S_{\alpha\beta}$ . Where polymer segments are aligned so that  $S_{\alpha\beta}$  is non-zero, other physical properties will be anisotropic as well. In particular the dielectric properties which determine the material refractive index will be affected, leading to the optical anisotropy known as birefringence. The correspondence of the stress tensor and the anisotropic part of the refractive index tensor is known as the ‘Stress-Optical Law’.

Kilfoil and Callaghan<sup>36</sup> have used deuterium nuclear magnetic resonance to measure the alignment tensor in a high molecular weight polymethylsiloxane (PDMS) melt, employing a small horizontal Couette cell (gap 0.5 mm) in which both the velocity axis element  $S_{xx}$  and the gradient element,  $S_{yy}$  of the alignment tensor can be projected along the magnetic field. In this work a small benzene probe molecule was placed as a dilute species near a polymer segment whose orientation  $\mathbf{u}$  defines the local director. The tumbling probe molecule undergoes steric interactions with that segment and experience an anisotropic mean orientation. The probe will thus exhibit a scaled down quadrupole splitting associated with that local site

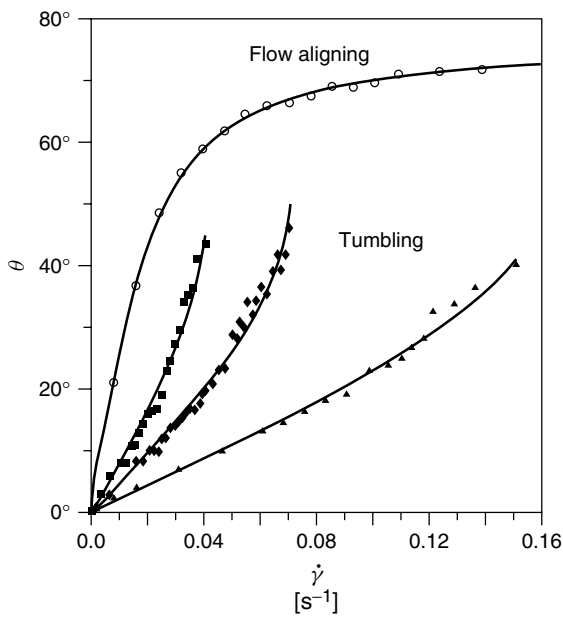


**Figure 10** Director orientation,  $\theta$  as a function of shear rate<sup>34</sup> for both flow aligning (solid squares) and tumbling (open squares 325 K, solid circles, 328 K and open circles 333 K) nematic polymers. (From Ref.<sup>34</sup>)

via a ‘pseudo-nematic’ interaction<sup>5</sup> and samples an ensemble average value for  $P_2(\cos\theta)$  as it diffuses over the molecular dimensions.

NMR micro imaging<sup>12</sup> is used to view the PDMS to image the velocity distribution across the gap while the selective-storage localized-spectroscopy method of Figure 3 is used to excite a desired region of the sample for spectroscopy experiments during steady-state shear. Figure 12 shows the measured alignment tensor elements along with fits using the Doi-Edwards model, in which the hierarchy of molecular relaxation times is terminated by the tube disengagement process associated with reptation. Also shown are the selected regions in which either the velocity direction or the velocity gradient (shear axis) is parallel to  $B_0$ . The selective excitation pulse sequence which we used has been specially devised to minimize exposure of selected nuclear spins to any relaxation. The best overall fit yields a tube disengagement time of 310 ms, a value which is consistent with the terminal relaxation rate obtained from mechanical measurements. We have also carried out this experiment<sup>36</sup> at fixed shear rate ( $\dot{\gamma}\tau_d = 3.9$ ), varying the angle  $\phi$  between the velocity direction  $X$  and the magnetic field direction through a number of prescribed angles. This was achieved by changing the orientation of the magnetic field gradient used in the precursor selective storage pulse. The angular dependence of the splitting is shown in

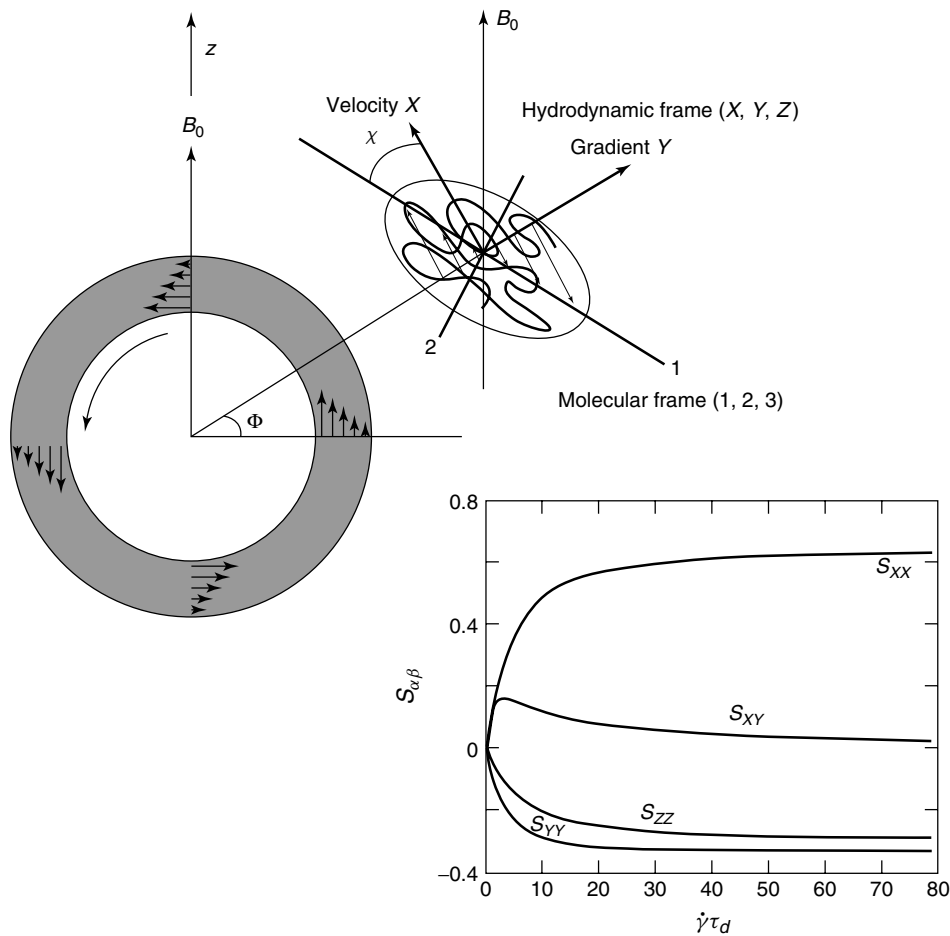


**Figure 11** Schematic diagram of ‘horizontal Couette cell’ in which the vorticity axis is aligned transverse to the magnetic field. The angle between the local velocity direction and the magnetic field is given by  $\phi$ . The angle between the principal axis of the molecular (1, 2, 3) frame and the velocity axis,  $X$ , is the so-called extinction angle  $\chi$ . The lower right inset shows elements of the alignment tensor,  $\dot{\gamma}\tau_d$

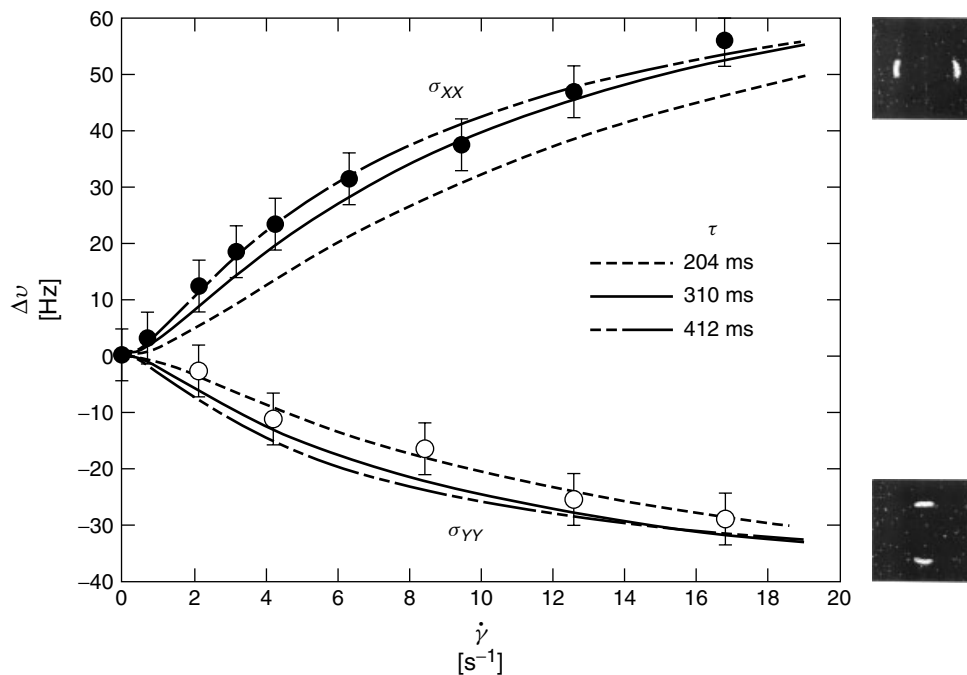


**Figure 12** Deuterium quadrupole splittings,  $\Delta v$ , versus shear rate, obtained<sup>36</sup> from the spectra derived from a selected region of the horizontal Couette cell in which the velocity direction (solid circles) and gradient direction (open circles) are respectively parallel to the magnetic field. The lines are fits using the Doi-Edwards model in which the absolute splitting (vertical axis) is scaled to yield the pseudonematic order parameter and the horizontal axis is scaled to yield the tube disengagement time,  $\tau_d$ . The best compromise fit corresponds to  $\tau_d = 310$  ms. The images at the right hand side show the regions selected for spectral investigation

Figure 13, along with the curve calculated using Doi-Edwards theory. Again the agreement is excellent, and consistent with the molecular principal axis being aligned at 14.6 degrees to the velocity axis.

### 3.4.2 $T_2$ Effects in Entangled Polymers and Gels

Another approach to Rheo-NMR has been demonstrated in a study of relaxation time effects in semi-dilute polymer

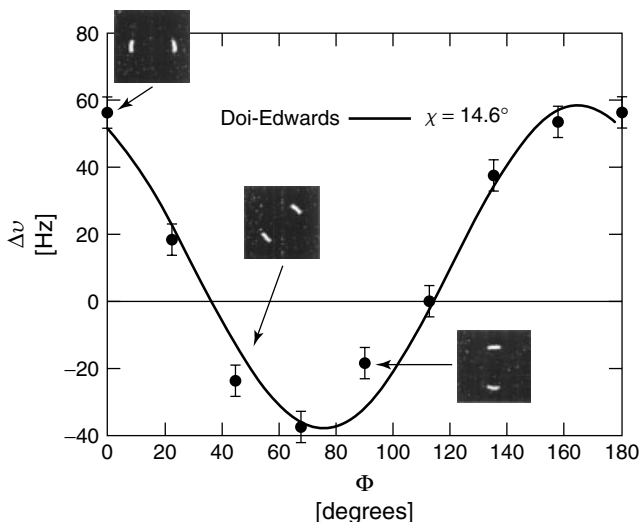


**Figure 13** Deuterium quadrupole splittings,<sup>36</sup>  $\Delta v$ , versus orientation angle,  $\phi$ , at a fixed Deborah number of  $\dot{\gamma}\tau_d = 3.9$ . The solid line shows the predictions of the Doi-Edwards model. The images show the selected regions used to obtain  $\phi = 0^\circ$ ,  $45^\circ$  and  $90^\circ$

solutions. Callaghan and Gil<sup>37</sup> used  $^1\text{H}$  spectroscopy to monitor  $T_2$  relaxation at selected sites on high molecular weight polyacrylamide (PAA) in water, using a cylindrical Couette cell. In this work micro-imaging was employed so that spatially dependent NMR parameters could be imaged across the shearing annulus. Shear banded flow was observed, and a marked reduction in polymer proton  $T_2$  values was found in the high shear region of the flow. Furthermore, the recovery of that  $T_2$  on shear cessation was indicative of slow reorganizational dynamics, on the order of tens to hundreds of seconds. The observed  $T_2$  recovery was found to be multi-exponential and the fast components correlated well with the terminal times measured from the steady state flow curve. Figure 14 shows the correlation of the shear banded flow and the relaxation time reduction while Figure 15 shows the recovery of the proton relaxation rate following shear cessation.

The relaxation effects have been interpreted as arising from a deformation of the entanglement tube, such that under strong shear a significant extension occurs along the velocity direction. In consequence, the curvilinear length around tube bends will increase, leading to a slower correlation time for the final orientational motional averaging step, and hence, a faster  $T_2$  relaxation rate.

In another experiment Callaghan and Gil<sup>38</sup> measured proton  $T_2$  relaxation in Carrageen gels under shear and have used changes in relaxation times to gain insight regarding intermolecular interactions responsible for gelation.  $T_2$  relaxation is a particularly easy NMR parameter to measure and may be equally easily used as a contrast in spatially resolved experiments. In consequence

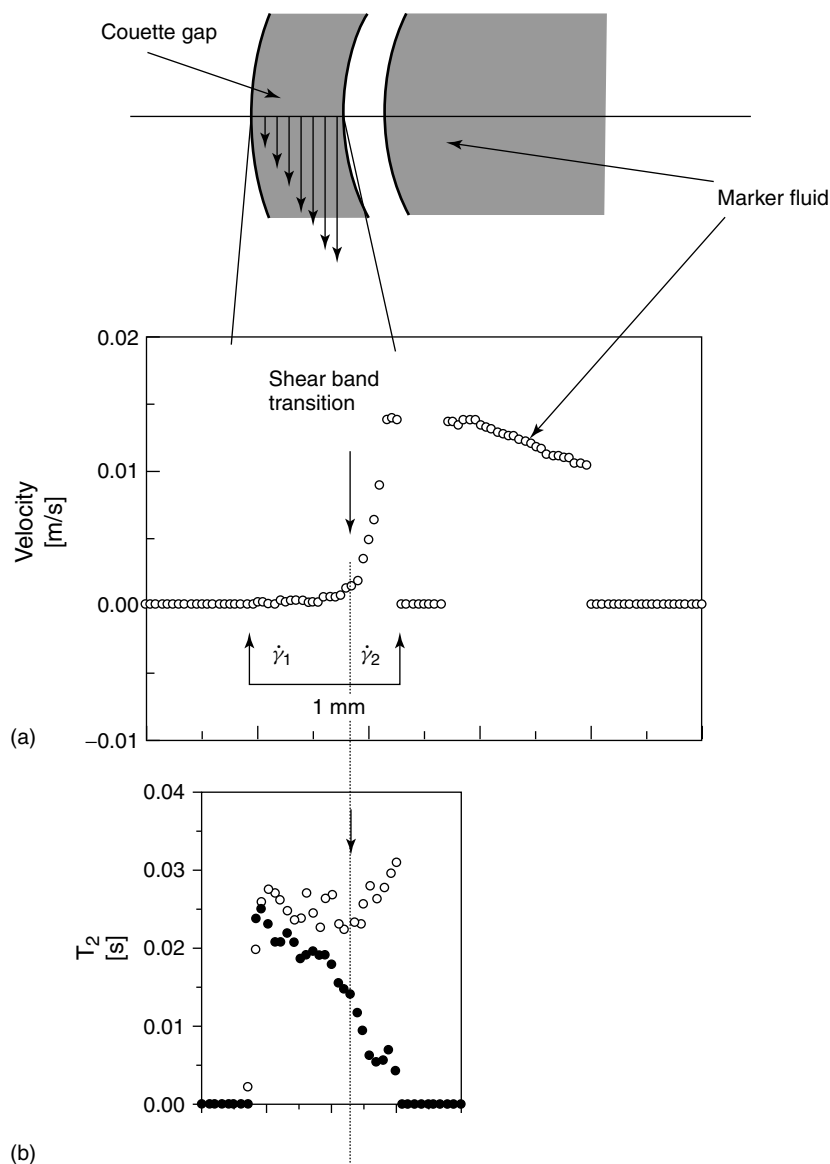


**Figure 14** Corresponding velocity and  $T_2$  profiles<sup>37</sup> of PAA/D<sub>2</sub>O as a function of radial position across the Couette cell annulus. The velocity profile was obtained at 0.50 Hz. The  $T_2$  profile with open circles is for zero shear and with closed circles for an inner cell rotation speed of 0.5 Hz. The horizontal scales of both velocity and  $T_2$  profiles are identical

the use of  $T_2$  perturbation as a probe of molecular conformational or organizational changes should prove a particularly useful tool in Rheo-NMR studies of complex fluids, and especially for those where changes occur sufficiently slowly that the  $T_2$  change can be observed as a transient.

### 3.5 Shear-induced Mesophase Structure

The potential for Rheo-NMR studies of shear-induced structure is considerable. One set of systems where NMR is ideally suited is that of lyotropic liquid crystalline phases. A range of cone and plate and cylindrical Couette cell studies have been reported by Lukashek et al.<sup>39,40</sup> and Müller et al.<sup>41</sup> These include cone-and-plate shearing of the hexagonal phase of the amphiphilic oligomer pentaoxyethylene monodecylether

(C<sub>12</sub>E<sub>5</sub> in D<sub>2</sub>O). Again, deuterium NMR quadrupolar splittings were used to give orientational information. The system appears to behave like a deformable solid, the final state at large strains corresponding to alignment of the hexagonal cylinders along the velocity axis.

For lamellar mesophases, a rich variety of structures is revealed by deuterium NMR studies under shear. For example in lamellar C<sub>12</sub>E<sub>4</sub> shear-aligned, defect-laden lamellae with directors perpendicular to the velocity direction form at low shear rates, but with a transition to spherical multi-lamellar vesicles taking place at higher shear rates. A wide range of lyotropic phases under shear have been studied using neutron scattering and X-ray scattering. NMR provides an opportunity to probe quite different length and time scales in these systems and should prove an important tool in elucidating the effect of deformational flow on molecular organization and dynamics.

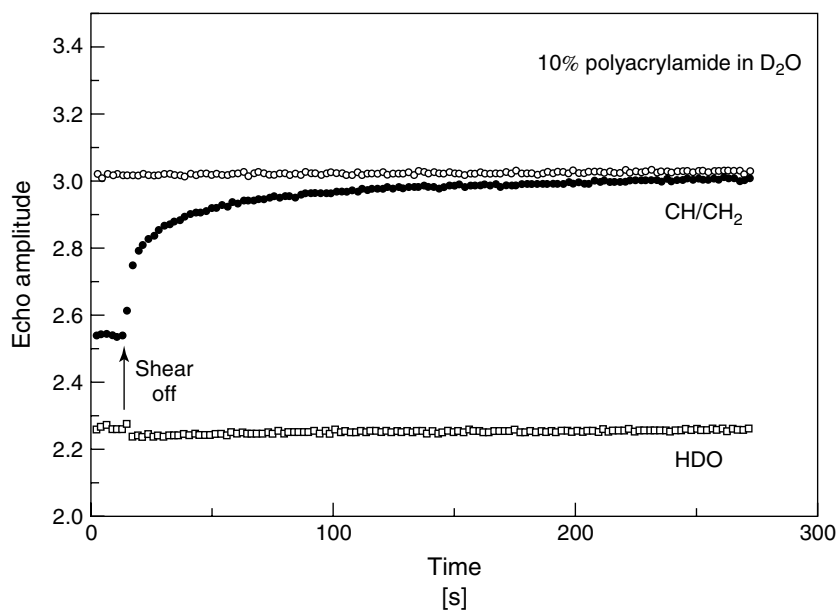


**Figure 15** Recovery of the spin echo signal<sup>37</sup> obtained at a fixed delay  $2\tau = 10$  ms for the CH/CH<sub>2</sub> region (solid circles) of the 300 MHz proton spectrum in 10% polyacrylamide in D<sub>2</sub>O. The open circles show the equilibrium baseline echo intensity obtained some minutes later after full relaxation. The behavior of the water (HDO) peak is shown. This exhibits a much weaker, but observable, transient effect, probably due to baseline effects arising from neighboring polymer proton resonances

### 3.6 Perturbing Intermolecular Interactions

Central to an understanding of the tertiary structure of biological macromolecules is the role of intermolecular interactions such as hydrogen bonds. Under shearing flow, molecules on differing local streamlines are separated, at a scale-independent rate given by  $\dot{\gamma}$ . If this rate exceeds the characteristic rate at which intermolecular bonds are naturally broken and reformed, then the tertiary structure is disrupted and the moieties responsible for bond formation will exhibit quite different dynamics than in the bonded state. Thus, Rheo-NMR provides a means of determining which sites on a molecule are responsible for intermolecular binding, by simply comparing high resolution NMR spectra obtained in states of equilibrium and under shear. An example a study of from the synovial fluid polysaccharide, hyaluronin,<sup>42</sup> where <sup>13</sup>C spectra have been compared. The one site which shows a significant change is that of the acetamido carbonyl, a moiety which is believed to be responsible for inter-molecular hydrogen bonding.

This last experiment makes clear the very general capability of the Rheo-NMR method. With the exception of the loss of sample space due to the presence of the central cylinder, no sacrifice in signal-to-noise ratio is made in order to carry out NMR under a shearing flow. The use of the cylindrical Couette cell, with all its faces (within the rf coil) machined parallel to the  $B_0$  field means that high spectral resolution is perfectly achievable. Consequently nearly all NMR spectroscopies that are possible in equilibrium, also are also possible under shear and this opens the way for a wide ranging series of NMR studies in which molecular sites responsible for intermolecular interactions are identified and their reaction dynamics determined.

### 3.7 Extensional Flow

Many important processes involving deformation of soft materials concern extensional flow. An example of an extensional flow cell is shown in Figure 16. The driving unit for this cell is programmed to move the top plug down and stop once the two plugs make contact, or, when a sample is present, when the sample has been deformed completely so as to fill the available volume. This action results in an increasing rate-of-strain,  $\dot{\epsilon}$ , as the two cylinders approach one another at velocity  $v$ , i.e.,

$$\dot{\epsilon} = \frac{v}{d_0 - vt} \quad (3)$$

where  $d_0$  is the gap at the time origin, chosen to be the point at which both surfaces come into contact with the material to be deformed. If we take the vertical (compression) axis as  $z$ , then the deformation tensor is diagonal and the flow may be ideally described by<sup>26</sup>

$$v_x = \frac{1}{2}\dot{\epsilon} \quad v_y = \frac{1}{2}\dot{\epsilon} \quad v_z = -\dot{\epsilon} \quad (4)$$

The sample generally takes the form of a semi-spherical blob of material. As a result, the final spacing of the plugs is determined by the point at which the material has spread to fill the available plug diameter. This device has been used to study the perturbation experienced in the proton spectrum of a polymer under deformation.<sup>43</sup>

## 4 CONCLUSIONS

These examples provide a glimpse of possible applications of Nuclear Magnetic Resonance to the study of complex fluid

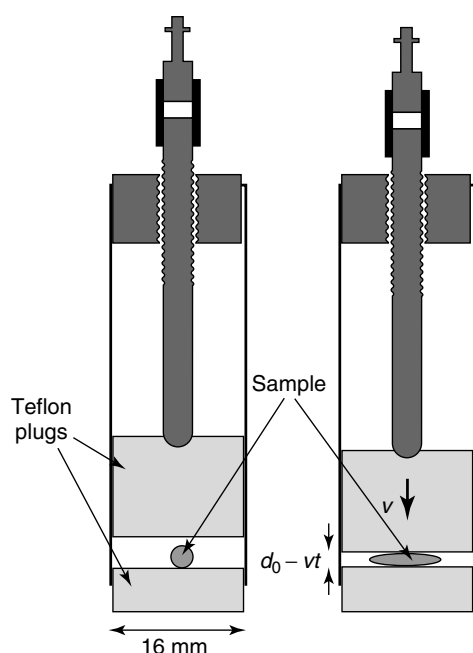


**Figure 16** Schematic diagram<sup>43</sup> of extensional flow cell with plug diameter 16 mm

rheology. While this is a very new field of research in which only a handful of groups presently participate, the potential exists for a substantial increase in Rheo-NMR research activity. Systems studied to date include polymer melts and semidilute solutions, thermotropic and lyotropic liquid crystals and liquid crystalline polymers, micellar solutions, food materials and colloidal suspensions. Rheo-NMR suffers in a number of respects by comparison with optical methods. NMR is an expensive and complex form of spectroscopy which requires familiarity with the nuclear spin Hamiltonian and the associated effects of spin dynamics. It often suffers from poor signal-to-noise ratios and requires careful tradeoffs in parameter space in order to optimize its effectiveness. Nonetheless NMR offers some unique advantages, including the ability to work with opaque materials, the ability to combine velocimetry with localized spectroscopy, and the ability to access a wide range of molecular properties relating to organization, orientation and dynamics. Rheo-NMR has been able to provide a direct window on a variety of behaviors, including slip, shear-thinning, shear banding, yield stress behavior, nematic director alignment and shear-induced mesophase reorganization. The unique information available with this method suggests that it is likely to become an important tool in elucidating the intriguing rheological behavior of a wide range of complex fluids.

## 5 REFERENCES

- H. A. Barnes, J. J. Hutton, and K. Walters, 'An Introduction to Rheology', Elsevier: Amsterdam, 1989.
- J. Kalus, G. Neubauer, and U. Schemlzer, *Rev. Sci. Instrum.*, 1990, **61**, 3384.
- R. J. Plano, C. R. Safinya, E. B. Sirota, and L. J. Wenzel, *Rev. Sci. Instrum.*, 1993, **64**, 1309.
- G. G. Fuller, *Annu. Rev. Fluid. Mech.*, 1990, **22**, 387.
- G. G. Fuller, 'Optical Rheometry of Complex Fluids', Clarendon Press: Oxford, 1995.
- A. F. Martins, P. Esnault, and F. Volino, *Phys. Rev. Lett.*, 1986, **57**, 1745.
- L. N. Goncalves, J. P. Casquilho, J. Figueirinhas, C. Cruz, and A. F. Martins, *Liquid Crystals*, 1993, **14**, 1485.
- A. I. Nakatani, M. D. Poliks, and E. T. Samulski, *Macromolecules*, 1990, **23**, 2686.
- Y. Xia and P. T. Callaghan, *Macromolecules*, 1991, **24**, 4777.
- D. A. Grabowski and C. Schmidt, *Macromolecules*, 1994, **27**, 2632.
- P. T. Callaghan, *Rep. Prog. Phys.*, 1999, **62**, 599.
- P. T. Callaghan, 'Principles of Nuclear Magnetic Resonance Microscopy', Oxford University Press: Oxford, 1991.
- E. O. Stejskal and J. E. Tanner, *J. Chem. Phys.*, 1965, **42**, 288.
- P. T. Callaghan, C. D. Eccles, and Y. Xia, *J. Phys. E*, 1988, **21**, 820.
- M. M. Britton, P. T. Callaghan, M. L. Kilfoil, R. W. Mair, and K. Owens, *Appl. Magn. Res.*, 1998, **15**, 287.
- R. Kimmich and D. Hoepfel, *J. Magn. Reson.*, 1987, **72**, 379.
- D. M. Doddrell, W. M. Brooks, J. M. Bulsing, J. Field, M. G. Irving, and H. Baddeley, *J. Magn. Reson.*, 1986, **68**, 367.
- H. Post, D. Ratzel, and P. Brunner, West German Patent, No. P3209263.6, 13 March 1982.
- W. P. Aue, S. Müller, T. A. Cross, and J. Seelig, *J. Magn. Reson.*, 1984, **56**, 350.
- M. L. Kilfoil and P. T. Callaghan, *J. Magn. Reson.*, 2000, in press.
- M. M. Britton and P. T. Callaghan, *Phys. Rev. Lett.*, 1997, **78**, 4930.
- M. E. Cates, *J. Phys. Chem.*, 1990, **94**, 371.
- M. E. Cates, T. C. B. McLeish, and G. Marrucci, *Europhys. Lett.*, 1993, **21**, 451.
- J. P. Decruppe, R. Cressely, R. Makhouffi, and E. Cappelaere, *Colloid Polymer Sci.*, 1995, **273**, 346.
- R. Makhouffi, J. P. Decruppe, A. Ait-Ali, and R. Cressely, *Europhys. Lett.*, 1995, **32**, 253.
- M. Doi and S. F. Edwards, 'The Theory of Polymer Dynamics', Oxford University Press: Oxford, 1987.
- E. Fischer and P. T. Callaghan, *Europhysics Lett.*, 2000, **50**, 803.
- F. M. Leslie, *Arch. Rat. Mech. Anal.*, 1968, **28**, 265.
- F. M. Leslie, *Q. J. Appl. Math.*, 1966, **19**, 357.
- J. L. Ericksen, *Arch. Rat. Mech. Anal.*, 1960, **4**, 231.
- J. L. Ericksen, *Trans. Soc. Rheol.*, 1961, **5**, 23.
- F. C. Frank, *Disc. Faraday Soc.*, 1958, **25**, 19.
- R. G. Larson, 'Constitutive Equations for Polymer Melts and Solutions', Butterworths: Boston, 1987.
- H. Siebert, D. A. Grabowski, and C. Schmidt, *Rheologica Acta*, 1997, **36**, 618.
- M. Doi and S. F. Edwards, *J. Chem. Soc. Faraday Trans. II*, 1978, **74**, 1802 and 1978, **74**, 1818.
- M. L. Kilfoil and P. T. Callaghan, *Macromolecules*, 2000, **33**, 6828.
- P. T. Callaghan and A. M. Gil, *Macromolecules*, 2000, **33**, 4116.
- P. T. Callaghan and A. M. Gil, in 'Magnetic Resonance in Food Systems', ed. G. A. Webb, Royal Society of Chemistry: London, 2000.
- M. Lukaschek, S. Müller, A. Hansenhindl, D. A. Grabowski, and C. Schmidt, *Colloid Polymer Sci.*, 1996, **274**, 1.
- M. Lukaschek, D. A. Grabowski, and C. Schmidt, *Langmuir*, 1995, **11**, 3590.
- S. Müller, P. Fischer, and C. Schmidt, *J. Phys II France*, 1997, **7**, 421.
- E. Fischer, P. T. Callaghan, F. Heatley, and J. E. Scott, *J. Mol. Struct.*, 2002, **303**, 602-603.
- P. T. Callaghan and A. M. Gil, *Rheologica Acta*, 1999, **38**, 528.

**Biographical Sketch**

Paul T. Callaghan received his D. Phil in Physics from Oxford University in 1974, having worked on low temperature studies of hyperfine interactions under the supervision of N. J. Stone. He is Professor of Physics at Massey University, New Zealand and heads a research team working on Pulsed Gradient Spin Echo NMR, and NMR microscopy studies of complex fluid dynamics, and flow and

dispersion in porous media. He is Alan MacDiarmid Professor of Physical Science at Victoria University of Wellington, New Zealand. He is author of the book 'Principles of Nuclear Magnetic Resonance Microscopy', published by Oxford University Press and has published around 170 articles in international scientific journals on the subject of nuclear magnetic resonance.